Chemically Inspired Convolutional Neural Network using Electronic Structure Representation

Dong Hyeon Mok[1†], Daeun Shin[2,3 †], Jonggeol Na[2,3] and Seoin Back[1]**

[1]Department of Chemical and Biomolecular Engineering, Institute of Emergent Materials, Sogang University, Seoul 04107, Republic of Korea

[2]Department of Chemical Engineering and Materials Science, Ewha Womans University, Seoul 03760, Republic of Korea

[3]Graduate Program in System Health Science and Engineering, Ewha Womans University, Seoul 03760, Republic of Korea

AUTHOR INFORMATION

Corresponding author(s)

E-mail: sback@sogang.ac.kr; jgna@ewha.ac.kr;

Contributing author(s)

E-mail: ahrehd0506@sogang.ac.kr; abcd990105@ewhain.net;

†These authors contributed equally to this work

Keywords

High-throughput screening, Thermodynamic stability, Density of states, Machine learning, Convolutional neural network

Abstract

In recent years, a development of appropriate crystal representations for accurate prediction of inorganic crystal properties has been considered as one of the essential tasks to accelerate materials discovery through high-throughput virtual screening (HTVS). However, many of them were developed aiming to predict properties of the given structures, although property predictions of ground state structures using unrelaxed structures as inputs are much more important in practical HTVS. To tackle this challenge, we develop a chemically inspired convolutional neural network based on convolution block attention modules using density of states of unrelaxed initial structures (IS-DOS) as inputs. Our model, Electronic Structure Network (ESNet), achieved the highest accuracy for predicting formation energy, proving that IS-DOS is appropriate input for the property prediction and the attention module is capable of properly featurizing DOS signals by capturing contributions of each spin and orbital state. In addition, we statistically evaluated a stability screening performance of ESNet, measuring computational cost and capability of materials discovery simultaneously. We found that ESNet outperformed previously reported models and various models with different types of input features and architectures. Indeed, ESNet successfully discovered 926 stable materials from 15,318 unrelaxed structures with 82 % reduced computational cost compared to the complete DFT validation.

Introduction

With increasing demands toward high-performing and cost-effective materials, it is becoming important to develop new strategies to accelerate an exploration of broad chemical space. The conventional approaches have relied on database corresponding to very small portion of chemical space, and time-consuming ab-initio calculations requiring huge computing resources[1]. Recently, various strategies to expand chemical space were developed, and machine learning (ML) has been utilized as powerful and efficient tools to facilitate materials discovery by reducing the number of required DFT calculations. In this aspect, fast and accurate ML models are desirable to enable high-throughput virtual screening (HTVS) of tens of thousands of materials[2, 3, 4].

Ideally, HTVS approaches explore all possible compounds in chemical space, which are generated by several methods such as elemental substitution and generative models[5]. Thus, one should develop ML models to directly predict ground state energies using unrelaxed initial structures, *i.e.*, initial structure to relaxed energy (IS2RE) task[6]. Graph neural networks (GNN), *e.g.,* crystal graph convolutional neural network (CGCNN)[7], are one of the most accurate and widely used approaches in the field, which describe local atomic environments of each atom in crystals as ML inputs[8, 9, 10]. They achieved very high accuracy for predicting crystal properties and can also be utilized to perform IS2RE task indirectly through numerical optimization algorithms, such as Broyden-Fletcher-Goldfarb-Shanno (BFGS)[11] or Bayesian optimization (BO)[12]. However, these are not suitable for practical HTVS since interatomic distances between neighboring atoms in relaxed structures are used to prepare input representations. Further, indirect IS2RE requires nearly 200 iterations of energy and force predictions for numerical geometry optimizations[6], and the predicted formation energy significantly depends on "pseudo" optimized structures, making IS2RE inefficient.[13, 14]. Direct IS2RE is also available with properly developed input representations such as direction, which is moderately sensitive to structures[13]. Meanwhile, a model which uses stoichiometry-based inputs achieved reasonable prediction accuracy,[15, 16, 17] but it was not able to distinguish polymorphs of materials. To accelerate materials discovery, it is thus necessary to develop accurate ML models for direct IS2RE with appropriate representations, neither too structure-sensitive nor too insensitive[13].

In this work, we report Electronic Structure Network (ESNet) based on convolutional neural network and convolution block attention modules (CBAM) using density of states (DOS)

of unrelaxed initial structures as input representations. Initially, we compared DOS of unrelaxed initial structures (IS) and relaxed structures (RS) to validate the use of IS-DOS for crystal structure representations, where we observed high similarity between IS-DOS and RS-DOS. By comparing with other models, we found that CBAM in ESNet successfully captures the contribution of DOS signal, representing each spin and orbital of crystal, to formation energy and ESNet is ideally suited to IS2RE task with the highest accuracy and efficiency. Furthermore, ESNet achieved both high success ratio and discoverability, breaking an inverse correlation between them[18]. The highest F_1-score of ESNet suggested that one can practically use this model for materials discovery via HTVS along with proper chemical space expansion approaches[19].

Results

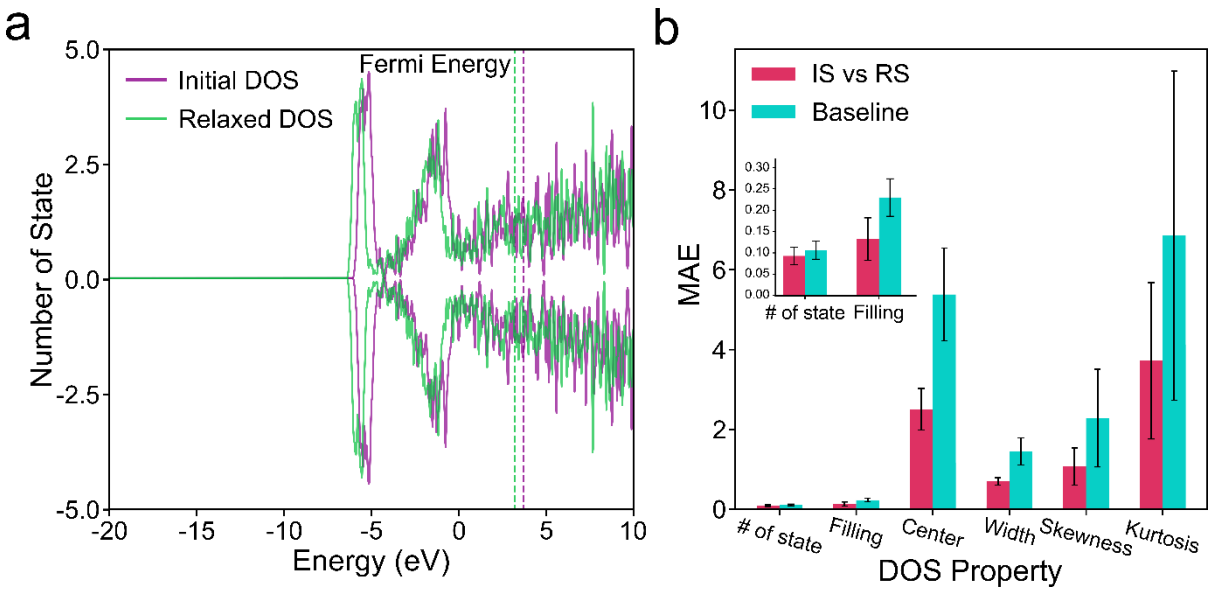

Figure 1. a) Total density of states of IS (purple) and RS (green) of CdAu constructed by substituting elements of PdHg (mp-2685). Dashed vertical lines correspond to the Fermi level of each structure. b) MAE of DOS properties between initial and relaxed structures (red), and between two random structures as a reference (turquoise). We measured MAEs of six DOS properties for 18 states, *i.e.,* nine orbitals (*s*, p_x, p_y, p_z, d_{xy}, d_{yz}, d_{xz}, $d_{x^2-y^2}$, d_{z^2}) × two spin states (*up* and *down* spins), where error bars correspond to standard deviations. Lower values indicate higher similarity.

DOS Similarity between Initial and Relaxed Structures

To corroborate the potential of IS-DOS as a proper representation of inorganic crystals

for IS2RE task, we compared similarities between DOS extracted from IS (IS-DOS) and RS (RS-DOS) (**Fig.1a**). We generated unrelaxed initial structures by substituting atoms in prototypical crystal structures taken from Materials Project. One can observe that a distribution of energy states remains unchanged even after the geometry relaxation. For a more quantitative comparison, we calculated the number of states per energy and 0−4th moment properties of DOS, *i.e.,* filling, center, width, skewness and kurtosis[20] for all crystal structures (7,168) in a validation set. We note that the number of states (*y*-axis of DOS) of each orbital and spin state was normalized using min-max normalization, and zero-state energy ranges were discarded to avoid an overestimation of similarity. As a baseline error, we randomly selected one IS-DOS and one RS-DOS from the validation set and calculated their similarities, 7,168 pairs in total. All similarity metrics between IS-DOS and RS-DOS were found to be significantly lower than the baseline errors (**Fig**.**1b**). From the qualitative and quantitative comparisons, we confirmed that DOS shapes and properties of initial and relaxed structures are similar, suggesting that IS-DOS could be proper crystal representations of ML models for IS2RE task. On the other hand, we note that bond distance information, which has been mainly utilized as inputs in various GNN models, changed significantly during the DFT relaxations, suggesting that it is inadequate to use distance-based features for IS2RE task (**Supplementary Fig.A1**)[13].

Deep Learning Model for Formation Energy Predictions

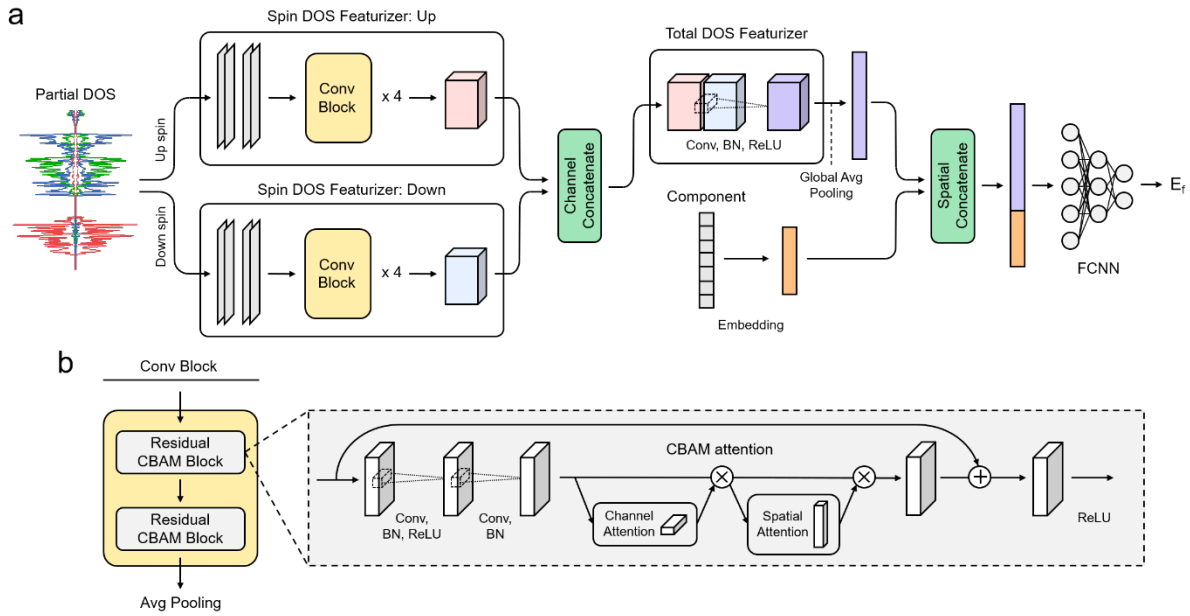

Figure 2. (a) Schematic representations of ESNet architecture. Partial DOS in each spin state and component vector are fed into the model as separate inputs. Three featurizers (up spin, down spin and total DOS featurizers) are used to generate total DOS feature maps from the input partial DOS. (b) Convolutional block architecture including two residual CBAM blocks. Through CBAM self-attention and residual connection, input feature maps autonomously learn weighted features. Each convolutional block is connected through average pooling.

In this work, we propose a deep learning model with a chemically inspired architecture optimized to featurize IS-DOS for accurate formation energy prediction. The model is based on convolutional neural network (CNN), which is suitable for high-level feature learning from multi-channel signal data[21, 22]. Since CNN takes inputs comprised of separate channels (orbitals) and featurizes the channels while preserving spatial information (spins), it is advantageous to featurize DOS consisting of various projected states. The featurized output (h_j^n) is updated as a sum of the product of convoluted input (h_k^{n-1}) and weight matrices (w_{kj}^n) (Eqn (1)).[21, 23]

$$h_j^n = \sum_{k=0}^{K} h_k^{n-1} \circ w_{kj}^n \quad (1)$$

The total DOS consists of two spin states and nine orbitals. We initially featurize each spin state using two spin DOS featurizers (**Fig.2a**),[24, 25] where each featurizer takes orbital projected DOS as inputs and extracts features based on the convolution operation (Eqn (2), (3)).

$$h_{j_{\mathrm{up}}}^{n} = \sum_{k_{\mathrm{up}}=0}^{K} h_{k_{\mathrm{up}}}^{n-1} \circ w_{k_{\mathrm{up}} j_{\mathrm{up}}}^{n} \tag{2}$$

$$h_{j_{\mathrm{down}}}^{n} = \sum_{k_{\mathrm{down}}=0}^{K} h_{k_{\mathrm{down}}}^{n-1} \circ w_{k_{\mathrm{down}} j_{\mathrm{down}}}^{n} \tag{3}$$

Note that two spin DOS featurizers are independent with different weight matrices. Spin DOS featurizer consists of four convolutional blocks which contain two residual convolutional block attention module (CBAM) blocks (**Fig.2b**)[26], intended to learn features effectively by focusing on important features (**Supplementary Fig.A2**)[26, 27]. The residual connection prevents loss of extracted features, which could occur due to the depth of models[28, 29]. After the subsequent convolutional blocks, total DOS feature maps of each spin state are obtained at the end of the featurizers, where they are concatenated and served as an input for total DOS featurizer. The total DOS featurizer aggregates the integrated feature maps of two spin states to form comprehensive feature maps covering all spin states and orbitals, which are then flattened and concatenated with the component vector. Finally, fully connected neural network (FCNN) is applied to predict formation energies. The key aspects of ESNet are its optimal operation for aggregation of partially projected DOS and chemically inspired architecture considering spin states and orbitals separately.

To train ESNet, we collected DFT-calculated DOS from Materials Project (MP) database[30]. In total, MP includes 62,842 materials, of which all orbitals have at least one spin state per energy for absolute energy range from −20 to 10 eV. We note that the dataset used in this work consist of only *s, p* and *d*-block elements, but it is possible to include *f*-block elements in training/test dataset by integrating extra channels in the model. Additionally, we highlight that our model could be universally used for formation energy prediction as it was trained with the dataset consisting of diverse compositions and crystal structures (**Supplementary Fig.A3 and Fig.A4**).

Prediction Performances

Table 1. Prediction performances of ML models with different input features and algorithms.

	RS2RE		IS2RE	
Model	MAE (eV/atom)	RMSE (eV/atom)	MAE (eV/atom)	RMSE (eV/atom)
DOS-free feature-based				
CGCNN-HD*	0.274	0.378	0.396	0.637
MEGNet*	0.256	0.353	0.369	0.592
Wren**	0.371	0.525	0.378	0.534
Roost***	0.429	0.617	0.429	0.617
DOS feature-based**				
KRR	0.271	0.435	0.338	0.527
SVR	0.280	0.446	0.442	0.655
RF	0.356	0.562	0.362	0.567
XGBoost	0.307	0.498	0.306	0.479
DNN	0.274	0.420	0.337	0.517
DOS signal-based				
CNN	0.273	0.397	0.301	0.436
ESNet (This work)	**0.232**	0.374	**0.265**	0.406

*Interatomic distances, **Wyckoff parameters, ***Stoichiometry

****0−4th moments (Filling, d-band center, Width, Skewness, Kurtosis), Compositions

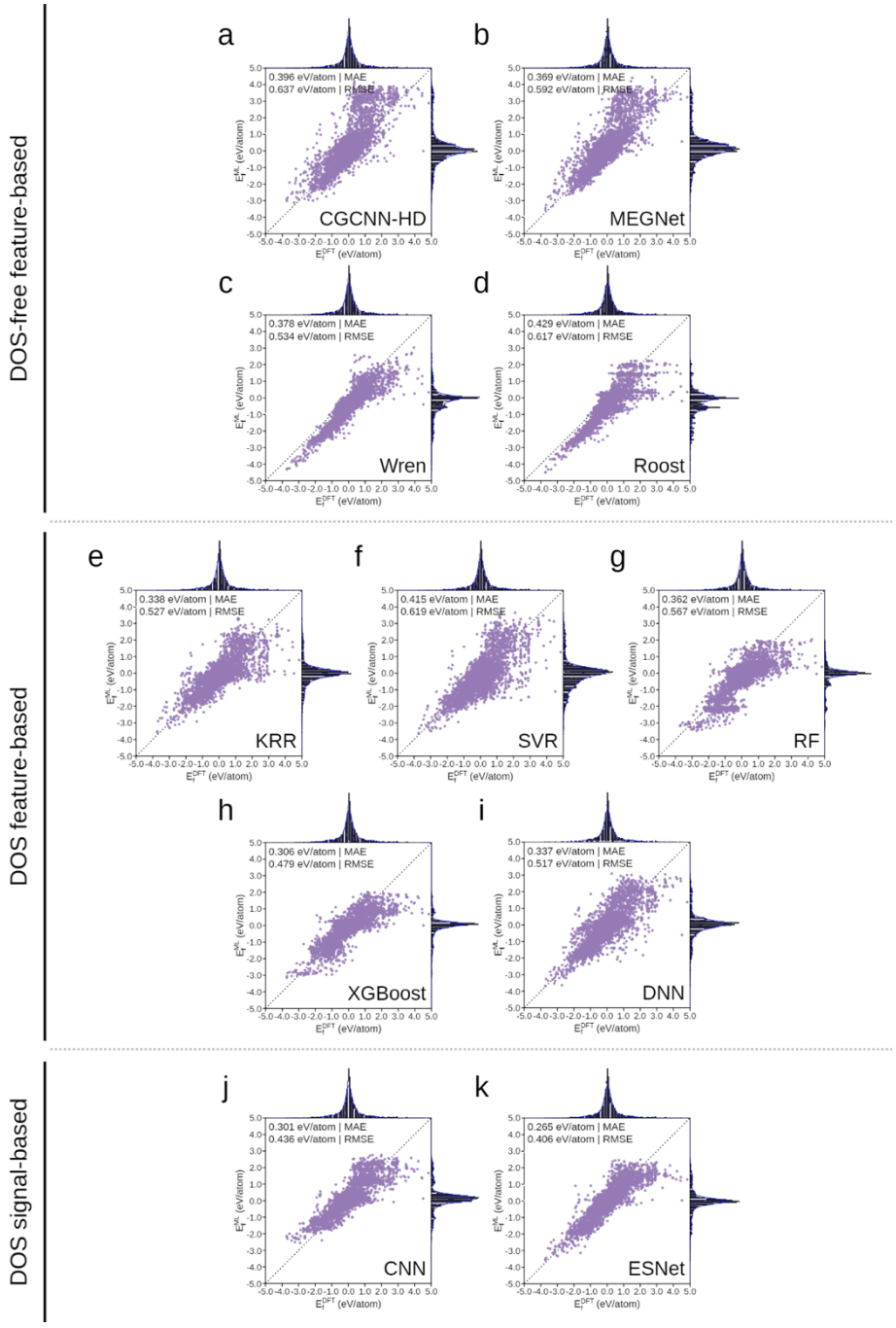

Figure 3. Parity plots of DFT-calculated and ML-predicted formation energies for IS2RE. Models are categorized into three groups depending on input types: (i) DOS-free feature-based, (ii) DOS feature-based and (iii) DOS signal-based models. DOS features are manually extracted features, *i.e.,* 0−4th moment properties, while DOS signal takes raw DOS data as inputs. Note that composition information was added to both DOS feature-based and DOS signal-based models. Test MAE and RMSE are shown.

We evaluated the prediction performance of ESNet and compared with other ML models based on different input features and algorithms (**Fig.3**). Although the focus of this work is IS2RE performance, we also discuss RS2RE results, which could be used in structure-to-energy and force (S2EF) mapping in the future[6]. For 7,168 test data (**Supplementary Fig.A5**), ESNet achieved higher performance for RS2RE (MAE: 0.232 eV/atom) than IS2RE (MAE: 0.265 eV/atom). Considering that training data consists of DOS and formation energies of relaxed structures, it is remarkable that the test MAE of IS2RE is close to that of RS2RE. We note that prediction performances of IS2RE and RS2RE are inversely correlated for the most previous models[31], but ESNet was able to break this correlation using IS-DOS as inputs, which substantially resemble RS-DOS.

For both IS2RE and RS2RE tasks, various models using different features and algorithms have been reported to date. We first compared ESNet with DOS-free feature-based models, *e.g.*, CGCNN-HD[32], MEGNet[8], Roost[15] and Wren[14], where the former two used interatomic distance-based features, while the latter two used coordinate-free features, such as stoichiometry (Roost) and Wyckoff positions (Wren) (**Fig.3a-d**). For IS2RE task, ESNet (Test MAE: 0.265 eV/atom) demonstrated the best prediction accuracy compared to all DOS-free ML models with MAEs larger than 0.35 eV/atom. It is noteworthy that prediction performances of RS2RE using MEGNet and CGCNN-HD were much higher than IS2RE, which could be mainly attributed to structure-sensitive input representations. On the contrary, Roost and Wren used structure-insensitive input representations that rarely distinguish IS and RS, resulting in nearly unchanged MAEs for IS2RE and RS2RE.

We also compared ESNet with other models (kernel ridge regressor (KRR)[33], support vector regressor (SVR)[34], random forest regressor (RFR)[35], XGBoost[36], deep neural network (DNN) with two fully connected layers[37, 38]) using extracted DOS features and composition information as inputs (**Fig.3e-i** and **Supplementary Table A1**). DOS feature-based models demonstrated higher prediction accuracy than DOS-free feature-based models, demonstrating the suitability of DOS as inputs for IS2RE. Interestingly, DOS-signal based models (ESNet and CNN) showed even higher accuracy, where ESNet particularly outperformed all ML models for both IS2RE and RS2RE (**Supplementary Fig.A6**). A comparison between DOS feature-based models and full DOS signal-based convolutional neural network models (ESNet, CNN[37, 39, 40]) demonstrates that only a few representative features are insufficient to properly describe properties of solid materials (**Fig.3j** and **k**). We further mention that ESNet outperformed the

conventional CNN, highlighting the importance of chemically inspired architecture and autonomously learned weights.

Screening Performances

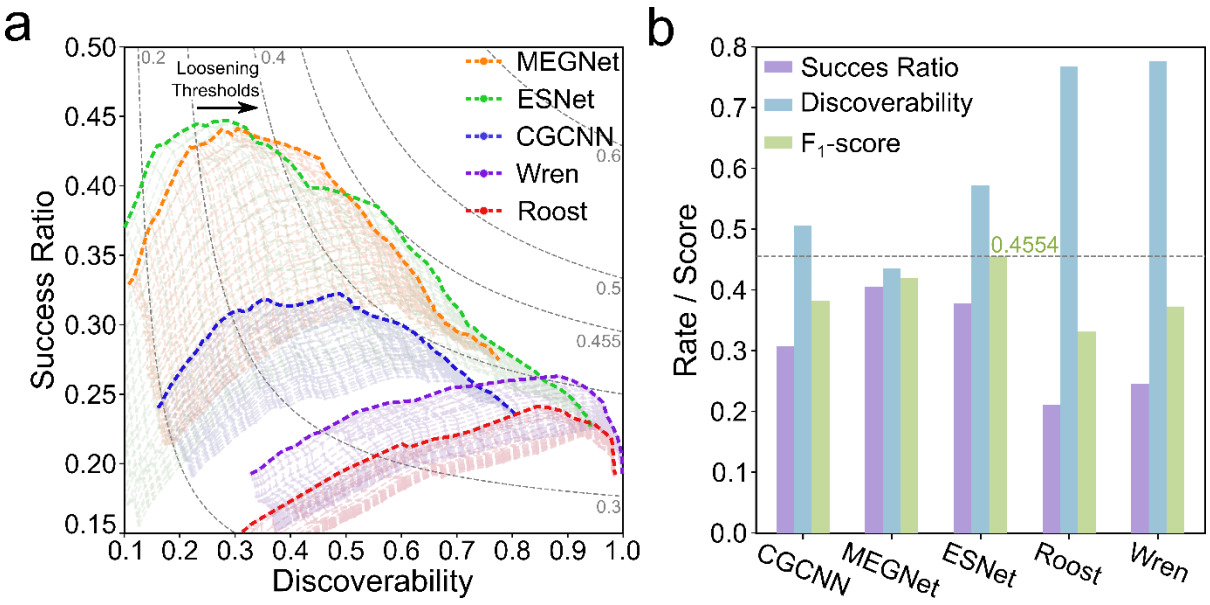

Figure 4. a) Two-dimensional precision-recall (P-R) curves generated by changing thresholds of E_f^{ML} and E_{hull}^{ML} from −0.25 to +0.25 eV/atom and 0.0 to +1.0 eV/atom, respectively. Right direction corresponds to loosening of E_f^{ML} and E_{hull}^{ML} thresholds. Gray dashed lines indicate different F_1-scores. b) Success ratio, discoverability and F_1-score of various models.

Given the best prediction accuracy of ESNet for IS2RE, we benchmarked its screening performance. Practically, ML models are employed in HTVS to determine whether new candidate materials are stable or not, thus classification metrics can be used to benchmark the screening performance[32].

The success ratio, or precision, is a ratio of DFT-validated stable materials among ML-predicted stable materials, and the discoverability, or recall, is a ratio of discovered stable materials by ML among all stable materials in the dataset (See "Terminology and Derivations of Statistical Metrics" in Method section for more details). To be suitable for HTVS, ML model should achieve both high success ratio and discoverability simultaneously. Thus, we not only evaluated these two metrics separately, but also at the same time using F_1-score, a harmonic

mean of two metrics[41, 42]. Note that we determined stability and synthesizability of materials when both formation energy (E_f^{DFT}) and energy above the convex hull (E_{hull}^{DFT}) satisfy criteria, $E_f^{DFT} \leq 0.0$ eV/atom and $E_{hull}^{DFT} \leq 0.1$ eV/atom, which are generally accepted thresholds in literature[7, 12, 43]. E_{hull}^{DFT} is calculated as formation energy difference with respect to the most stable phase at that composition. Thresholds of E_f^{ML} and E_{hull}^{ML}, however, are set by researchers' intuition and prediction accuracy of ML models, which could significantly affect HTVS results. Thus, we tested numerous values of E_f^{ML} (from −0.25 to +0.25 eV/atom) and E_{hull}^{ML} (from 0.0 to +1.0 eV/atom) to find the optimal combination to maximize the F_1-score for an efficient and accurate screening. We note that E_{hull}^{ML} was obtained by incorporating E_f^{ML} into a pool of inorganic solid materials in MP database using the Pymatgen library.

Precision-Recall (P-R) curve is commonly employed to evaluate classification performances, where the upper right corner corresponds to better screening results (**Fig.4a**)[41, 44]. To clearly understand the trends, we visualized the effect of changing thresholds of E_f^{ML} and E_{hull}^{ML} in three dimensions (**Supplementary Fig.A7**). For all models, we found that success ratio and discoverability are proportional to each other when E_{hull}^{ML} is lower than ~0.1 eV/atom, while they become inversely proportional otherwise. Thus, the maximum F_1-score for all models was achieved near E_{hull}^{ML} = 0.1 eV/atom (**Supplementary Table A2**). Among all models, ESNet achieved the best F_1-score when $E_f^{ML} \leq -0.02$ eV/atom and $E_{hull}^{ML} \leq 0.13$ eV/atom thresholds were used.

Figure 4b summarizes three metrics at the optimal threshold values for each ML model. CGCNN-HD and MEGNet demonstrated a high success ratio, but low discoverability, which could be linked to the behavior observed in **Figure 4a**, where the curves lean to the upper left. This is because ML models using distance-based features tend to overestimate E_f and E_{hull} (**Fig.3a, 3b)** resulting in a small number of ML-predicted stable materials, making success ratio high and discoverability low. In this case, a large portion of stable materials could not be discovered. Conversely, Wren and Roost are positioned at the lower right, demonstrating low success ratio and high discoverability. This is because they tend to underestimate E_f and E_{hull} (**Fig.3c** and **3d)**. Thus, many ML-predicted stable materials resulted in a low success ratio and high discoverability. Contrary to these two cases, ESNet achieved a balance between success ratio and discoverability, maximizing F_1-score (**Fig.4b**). This could also be evidenced by the P-R curve, where points of ESNet are positioned toward upper right compared to any other ML models (**Fig.4a**). In this analysis, we confirmed that ESNet is most suitable for IS2RE, thus, in

the following, we performed HTVS to find stable materials using ESNet.

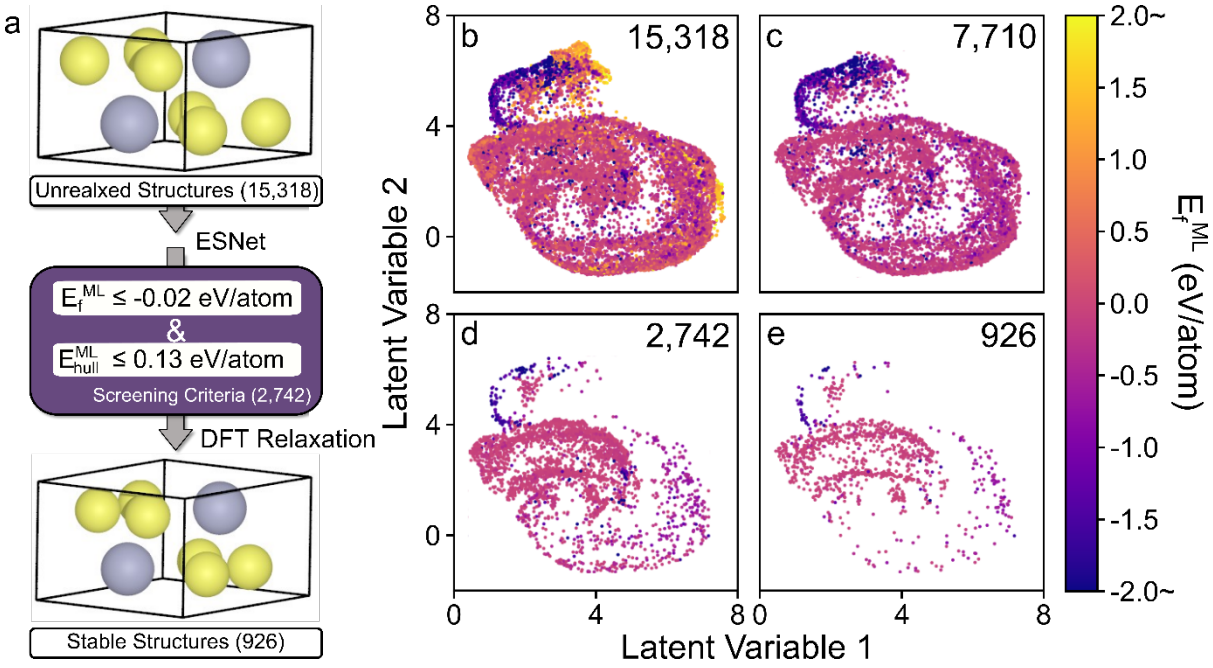

Figure 5. (a) Schematic representation of HTVS and (b)-(e) latent space generated by UMAP[45] visualizing HTVS process to discover stable materials. A color bar corresponds to E_f^{ML} predicted by ESNet. (b) The predicted formation energy of the remaining unrelaxed 15,318 materials. In (c)-(e), only materials satisfying the following conditions are plotted in the latent space. (b) 7,710 structures satisfied $E_f^{ML} \leq -0.02$ eV/atom. (c) 2,742 structures additionally satisfied $E_{hull}^{ML} \leq 0.13$ eV/atom. (d) 2,742 structures were optimized and 926 were found to satisfy both $E_f^{DFT} \leq 0$ eV/atom and $E_{hull}^{DFT} \leq 0.1$ eV/atom.

High-Throughput Virtual Screening

Using ESNet trained with 62,842 data from MP database, we performed HTVS to discover stable materials. Note that the optimal thresholds of E_f^{ML} and E_{hull}^{ML} determined for ESNet were used to maximize F_1-score. We applied ESNet to 2e-ORR dataset to discover stable unrelaxed structures, where more details on the dataset can be found in the method section. Out of 22,709 total bulk structures, 7,168 structures were relaxed and used for validation of ML models, thus formation energies of 15,318 unrelaxed structures were predicted (**Fig.5a**). To visualize the screening process and distribution of E_f^{ML} of 2e-ORR dataset, we used uniform manifold approximation and projection (UMAP)[45] which reduces the dimension of input DOS into two dimensions (**Fig.5b-e**). Initially, 7,710 structures satisfied $E_f^{ML} \leq -0.02$ eV/atom, and

only 2,742 structures additionally satisfied $E_{hull}^{ML} \leq 0.13$ eV/atom. Thus, negative E_{hull}^{ML} indicates that materials are predicted to be more stable than the existing most stable material in MP database. Finally, DFT relaxations were performed to validate 2,742 materials, where 926 materials satisfied both $E_f^{DFT} \leq 0$ eV/atom and $E_{hull}^{DFT} \leq 0.1$ eV/atom. This result demonstrates that ESNet found 926 stable and synthesizable materials by performing only 18 % of DFT calculations.

Discussions and Conclusions

In this work, we found that DOS-based input representations are more accurate for predicting the ground state stability than any other DOS-free feature-based models. However, one should perform single-point calculations to generate DOS, which could be a bottleneck in terms of computational cost as the number of materials increases.

To compare the computational cost used for screening, we defined a screening efficiency (C_{eff}) as

$$C_{eff} = \frac{C_{opt} * PPCR + C_{pre}}{Discoverability} \quad (4)$$

where C_{opt} and PPCR (predicted positive condition rate) are the average CPU time used for structure relaxations (3107.000 sec) and the ratio of the predicted stable materials to the total data set (15,318) for each model, respectively. C_{pre} is the average CPU time used for DOS generation (108.506 sec), which only applies to ESNet (**Supplementary Fig.A8a** and **b**). C_{eff} is, thus, a ratio of the total CPU time consumption per discovered stable materials, where lower C_{eff} suggests higher screening efficiency. **Supplementary Fig.A8c** and **d** show C_{eff} of each model with respect to threshold values for E_f^{ML} and E_{hull}^{ML}, respectively. This result indicates that C_{eff} of ESNet is similar to that of CGCNN, but preceded by MEGNet, indicating that the efficiency of ESNet is not the best. Considering the highest F_1-score and moderate C_{eff} even with single-point calculations of all initial structures for DOS generation, however, we propose ESNet to be the most practical ML model for HTVS.

In summary, we developed the deep learning model to predict thermodynamic stability of inorganic crystal structures using density of states of unrelaxed initial structures as input representations, and benchmarked its prediction accuracy and screening performance with

respect to the previously reported ML models. ESNet demonstrated the highest prediction accuracy for both IS2RE and RS2RE, where test set MAE of IS2RE (0.265 eV/atom) was found to be outstanding compared to other models (0.378~0.429 eV/atom). By optimizing thresholds of E_f^{ML} and E_{hull}^{ML}, we determined the best combination for each model to maximize F_1-score. Among all models, ESNet achieved the highest F_1-score, indicating the best screening performance, while its computational cost was comparable to the most efficient ML model even with additional calculations for DOS construction. These results demonstrated that ESNet is best suited to IS2RE task.

Method

DFT Calculations

To generate density of states of initial structures (IS-DOS) and conduct geometry optimizations, we performed spin-polarized density functional theory (DFT) calculations with generalized gradient approximation Perdew-Burke-Ernzerhof (GGA-PBE) exchange-correlation functional[46] using Vienna Ab initio Simulation Package (VASP, version 5.4.4)[47, 48]. Since training data, *i.e.,* DOS and E_f, were taken from Materials Project (MP) database, a compatible version (v2010-05-06) of projected augmented wave (PAW) pseudopotential was used. The energy cutoff, energy and force convergence criteria for bulk optimizations were set to 520 eV, 10^{-5} eV and 0.03 eV/Å, respectively. Monkhorst-Pack k-point mesh of ($k_1 \times k_2 \times k_3$) was set so that $a_n \times k_n$ ($n = 1, 2, 3$) ≥ 30, where a_1, a_2 and a_3 are lattice parameters of *x, y* and *z* directions of the unit cell, respectively[49]. DOS was obtained with VASP tags set to EMIN = −20 eV, EMAX = 10 eV and NEDOS = 1,500.

Data Generation

In MP database, 74,922 materials were deposited with their DFT-calculated DOS information as of 2021-03-22. Among them, we collected 62,842 materials consisting of *s, p, d*-orbitals, which were used to train ESNet. Mean and standard deviation of formation energy (E_f^{DFT}) were −1.407 and 1.101 eV/atom, respectively, where it ranged from −13.577 to 5.146 eV/atom (**Supplementary Fig.A4**).

DOS information in MP database has different energy ranges depending on materials, where the number of energy intervals was equivalently set to 2,001. Thus, energy values were interpolated using "interp1d" function of "scipy" library, so that all materials are represented by DOS of the same energy range (−20 eV ~ 10 eV) and resolution (0.02 eV). When no state is available in that energy range, it was set to be 0. For materials with only one spin state, the other spin state was set to be identical with the opposite sign. To evaluate the performance of ESNet, we used electrochemical two-electron O_2 reduction reaction (2e-ORR) dataset, which contains 22,709 binary alloys generated by elemental substitution of MP database. More details of 2e-ORR dataset can be found in https://github.com/SeoinBack.

Data Preprocessing

We generated input representations using the calculated IS-DOS, which consist of up and down spin states of 9 orbitals from *s* to *d* (*s, p_x, p_y, p_z, d_{xy}, d_{yz}, d_{xz}, d_{x2-y2}, d_{z2}*). When DOS signals are directly used in convolutional neural networks, each one comprises an individual input channel (total 18 channels), where StandardScaler was applied to remove the mean and to scale to unit variance. After preprocessing 18 channels, we added one extra channel representing a composition of materials, where one-hot encoding of all the elements in our dataset, 110, was used.

As a comparison, we also constructed DOS feature vectors consisting of 0−4th moment properties of DOS, thus 90 features in total considering 5 moment properties and 18 orbitals. In addition, the identical one-hot encoded composition vector was concatenated.

Terminology and Derivation of Metrics

To evaluate screening performances of ML models, we used statistical metrics derived from a confusion matrix[50]. We considered positive (P) and negative (N) to be stable and unstable, respectively, where stable materials satisfy criteria for both E_f^{DFT} and E_{hull}^{DFT}. On this basis, success ratio, same as precision or positive predictive value (PPV), is defined as TP / (TP + FP), where true positive (TP) is the number of DFT-validated stable materials, whereas false positive (FP) is the number of ML-predicted stable materials that are found to be unstable by DFT validations. ML models with high success ratio are suited to minimize unnecessary computational expenses caused by false positive. Discoverability, equivalent to recall or true positive rate (TPR), is defined as TP / (TP + FN), where false negative (FN) is the number of stable materials incorrectly predicted to be unstable. Thus, ML models with high discoverability are useful for reducing the number of overlooked candidates.

Model Implementation and Training

ESNet learns nonlinear relationship between DOS and formation energy. The model receives three types of inputs, up/down spin states with 9 channels (orbitals) and a binary component represented by one-hot vector. The inputs pass four main parts composing the model: (1) spin DOS featurizer, (2) total DOS featurizer, (3) component embedding, and (4)

formation energy predictor. In the spin DOS featurizer, each spin state of input DOS is fed separately into 1D convolutional neural network (1D CNN) with convolutional block attention modules (CBAM) and residual connection added. For example, in the case of up spin state, there are four convolution blocks, where each block consists of two convolution units. The units sequentially use two 1D convolutional layers, followed by a CBAM and a residual connection. Pooling layers are placed before moving from one block to the next. The convolution kernel sizes are fixed to 3, and the number of kernels is set to 64, 128, 256, and 512 per block, respectively. Down spin state also has the same architecture as above. The outputs of each convolutional network, which correspond to up and down spin states, are concatenated, and they pass through a convolutional layer with 512 kernels with a size of 3 in the total DOS featurizer. The output of the last convolutional layer is downsampled using the global average pooling layer. Meanwhile, the input component vector is embedded into a vector of length 50 through a fully connected layer without activation functions. Finally, the downsampled vector and embedded vector are concatenated on the length dimension and then predict the formation energy through fully connected layers as the predictor. All layers, whose activation is not specified explicitly, used rectified linear unit (ReLU) activations. The entire model has 9,756,225 total parameters and 9,736,001 trainable parameters. Tensorflow 2.4.1 and Keras 2.4.0 are used as the backend for the model implementation.

In this work, the model performance showed a relatively high dependence on initial learning rate (init_lr) and batch size (bs). Thus, a hyperparameter optimization was performed with these two hyperparameters using both manual grid search and Bayesian optimization implemented in Ax through Ray package[51]. The hyperparameter space for init_lr and bs is set to be an integer from 16 to 65, and a float from 0.0005 to 0.002, respectively. The best performance was achieved when init_lr = 0.00175 and bs = 32. We used Adam optimizer with the optimized initial learning rate of 0.00175 and learning rate schedule with plateau detection for learning rate reduction. The model was trained for 300 epochs with an early stopping algorithm on an NVIDIA GPU with memory and CUDA 11.0. The LogCosh function is selected as the loss function due to the robustness of possible outliers in high throughput databases and the precision that continuous differentiation is possible even in low errors. Mean absolute errors (MAE) and root mean squared errors (RMSE) are chosen to evaluate model performances.

Data availability

The raw data used in this work will be available at https://github.com/SeoinBack/.

Code availability

The machine learning code developed in this work will be available at https://github.com/

Acknowledgements

We acknowledge the financial support from National Research Foundation of Korea (NRF-2015M3D3A1A01064929, NRF-2021R1C1C1012031).

Author contributions

D.H.M. and S.B. conceptualized the project. S.B. and J.N. supervised the project. D.H.M. conducted DFT calculations. D.S. constructed machine learning model. All the authors discussed the results and wrote the manuscript.

Competing interests

The authors declare no competing interests

Supplementary information

Supplementary Figure 1 – 8, Supplementary Table 1 – 2

References

1. Pyzer-Knapp EO, Suh C, Gómez-Bombarelli R, Aguilera-Iparraguirre J, Aspuru-Guzik A. What is high-throughput virtual screening? A perspective from organic materials discovery. *Annu Rev Mater Res*, (2015).

2. Tran K, Ulissi ZW. Active learning across intermetallics to guide discovery of electrocatalysts for CO 2 reduction and H 2 evolution. *Nat Catal* **1**, 696-703 (2018).

3. Gu GH, Noh J, Kim I, Jung Y. Machine learning for renewable energy materials. *Journal of Materials Chemistry A* **7**, 17096-17117 (2019).

4. Mok DH, Back S. Atomic Structure-free Representation of Active Motifs for Expedited Catalyst Discovery. *J Chem Inf Model* **61**, 4514-4520 (2021).

5. Noh J, Gu GH, Kim S, Jung Y. Machine-enabled inverse design of inorganic solid materials: promises and challenges. *Chemical Science* **11**, 4871-4881 (2020).

6. Chanussot L*, et al.* Open catalyst 2020 (OC20) dataset and community challenges. *ACS Catal* **11**, 6059-6072 (2021).

7. Xie T, Grossman JC. Crystal graph convolutional neural networks for an accurate and interpretable prediction of material properties. *Phys Rev Lett* **120**, 145301 (2018).

8. Chen C, Ye W, Zuo Y, Zheng C, Ong SP. Graph networks as a universal machine learning framework for molecules and crystals. *Chem Mater* **31**, 3564-3572 (2019).

9. Shuaibi M*, et al.* Rotation invariant graph neural networks using spin convolutions. *arXiv preprint arXiv:210609575*, (2021).

10. Gasteiger J, Becker F, Günnemann S. Gemnet: Universal directional graph neural networks for molecules. *Adv Neural Inf Process Syst* **34**, 6790-6802 (2021).

11. Head JD, Zerner MC. A Broyden—Fletcher—Goldfarb—Shanno optimization procedure for molecular geometries. *Chem Phys Lett* **122**, 264-270 (1985).

12. Zuo Y*, et al.* Accelerating materials discovery with Bayesian optimization and graph deep learning. *Materials Today* **51**, 126-135 (2021).

13. Mok DH, Kim J, Back S. Direction-based Graph Representation to Accelerate Stable Catalysts Discovery. (2022).

14. Goodall RE, Parackal AS, Faber FA, Armiento R, Lee AA. Rapid Discovery of Novel Materials by Coordinate-free Coarse Graining. *arXiv preprint arXiv:210611132*, (2021).

15. Goodall RE, Lee AA. Predicting materials properties without crystal structure: Deep representation learning from stoichiometry. *Nat Commun* **11**, 1-9 (2020).

16. Meredig B*, et al.* Combinatorial screening for new materials in unconstrained composition space with machine learning. *Phys Rev B* **89**, 094104 (2014).

17. Wang AY-T, Kauwe SK, Murdock RJ, Sparks TD. Compositionally restricted attention-based network for materials property predictions. *Npj Comput Mater* **7**, 1-10 (2021).

18. Buckland M, Gey F. The relationship between recall and precision. *Journal of the American society for information science* **45**, 12-19 (1994).

19. Lipton ZC, Elkan C, Naryanaswamy B. Optimal thresholding of classifiers to maximize F1 measure. In: *Joint European Conference on Machine Learning and Knowledge Discovery in Databases*). Springer (2014).

20. Nørskov JK, Studt F, Abild-Pedersen F, Bligaard T. *Fundamental concepts in heterogeneous catalysis*. John Wiley & Sons (2014).

21. Kiranyaz S, Ince T, Abdeljaber O, Avci O, Gabbouj M. 1-D convolutional neural networks for signal processing applications. In: *ICASSP 2019-2019 IEEE International Conference on Acoustics, Speech and Signal Processing (ICASSP)*). IEEE (2019).

22. Fung V, Hu G, Ganesh P, Sumpter BG. Machine learned features from density of states for accurate adsorption energy prediction. *Nat Commun* **12**, 1-11 (2021).

23. Chen Y. Convolutional neural network for sentence classification.). University of Waterloo (2015).

24. Mavropoulos P, Sato K, Zeller R, Dederichs P, Popescu V, Ebert H. Effect of the spin-orbit interaction on the band gap of half metals. *Phys Rev B* **69**, 054424 (2004).

25. Yeo BC, Kim D, Kim C, Han SS. Pattern learning electronic density of states. *Scientific reports* **9**, 1-10 (2019).

26. Woo S, Park J, Lee J-Y, Kweon IS. Cbam: Convolutional block attention module. In: *Proceedings of the European conference on computer vision (ECCV)*) (2018).

27. Yadav S, Rai A. Frequency and temporal convolutional attention for text-independent speaker recognition. In: *ICASSP 2020-2020 IEEE International Conference on Acoustics, Speech and Signal Processing (ICASSP)*). IEEE (2020).

28. He K, Zhang X, Ren S, Sun J. Deep residual learning for image recognition. In: *Proceedings of the IEEE conference on computer vision and pattern recognition*) (2016).

29. Du X, Liao K, Shen X. Secondary radar signal processing based on deep residual separable neural network. In: *2020 IEEE International Conference on Power, Intelligent Computing and Systems (ICPICS)*). IEEE (2020).

30. Jain A*, et al.* Commentary: The Materials Project: A materials genome approach to accelerating materials innovation. *APL Mater* **1**, 011002 (2013).

31. Gibson J, Hire A, Hennig RG. Data-augmentation for graph neural network learning of the relaxed energies of unrelaxed structures. *Npj Comput Mater* **8**, 1-7 (2022).

32. Noh J, Gu GH, Kim S, Jung Y. Uncertainty-quantified hybrid machine learning/density functional theory high throughput screening method for crystals. *J Chem Inf Model* **60**, 1996-2003 (2020).

33. Schölkopf B, Smola AJ, Bach F. *Learning with kernels: support vector machines, regularization, optimization, and beyond*. MIT press (2002).

34. Awad M, Khanna R. Support vector regression. In: *Efficient learning machines*). Springer (2015).

35. Breiman L. Random forests. *Machine learning* **45**, 5-32 (2001).

36. Chen T, Guestrin C. Xgboost: A scalable tree boosting system. In: *Proceedings of the 22nd acm sigkdd international conference on knowledge discovery and data mining*) (2016).

37. LeCun Y, Bengio Y, Hinton G. Deep learning. *nature* **521**, 436-444 (2015).

38. Goodfellow I, Bengio Y, Courville A. *Deep learning*. MIT press (2016).

39. Simonyan K, Zisserman A. Very deep convolutional networks for large-scale image recognition. *arXiv preprint arXiv:14091556*, (2014).

40. Sun D, Chen Y, Liu J, Li Y, Ma R. Digital signal modulation recognition algorithm based on vggnet model. In: *2019 IEEE 5th international conference on computer and communications (ICCC)*). IEEE (2019).

41. Zhang Y*, et al.* Development of an automated screening system for retinopathy of prematurity using a deep neural network for wide-angle retinal images. *IEEE access* **7**, 10232-10241 (2018).

42. Rachman A, Ratnayake RC. Machine learning approach for risk-based inspection screening assessment. *Reliability Engineering & System Safety* **185**, 518-532 (2019).

43. Sun W*, et al.* The thermodynamic scale of inorganic crystalline metastability. *Sci Adv* **2**, e1600225 (2016).

44. Davis J, Goadrich M. The relationship between Precision-Recall and ROC curves. In: *Proceedings of the 23rd international conference on Machine learning*) (2006).

45. McInnes L, Healy J, Melville J. Umap: Uniform manifold approximation and projection for dimension reduction. *arXiv preprint arXiv:180203426*, (2018).

46. Hammer B, Hansen LB, Nørskov JK. Improved adsorption energetics within density-functional theory

using revised Perdew-Burke-Ernzerhof functionals. *Phys Rev B* **59**, 7413 (1999).

47. Kresse G, Hafner J. Ab initio molecular dynamics for open-shell transition metals. *Phys Rev B* **48**, 13115 (1993).

48. Kresse G, Furthmüller J. Efficiency of ab-initio total energy calculations for metals and semiconductors using a plane-wave basis set. *Comput Mater Sci* **6**, 15-50 (1996).

49. Monkhorst HJ, Pack JD. Special points for Brillouin-zone integrations. *Phys Rev B* **13**, 5188 (1976).

50. Fawcett T. An introduction to ROC analysis. *Pattern recognition letters* **27**, 861-874 (2006).

51. Moritz P*, et al.* Ray: A distributed framework for emerging {AI} applications. In: *13th USENIX Symposium on Operating Systems Design and Implementation (OSDI 18)*) (2018).